Advanced Composites and Hybrid Materials (2021) 4:534–542
https://doi.org/10.1007/s42114-021-00242-z

ORIGINAL RESEARCH

Tunable positive magnetoresistance of magnetic polyaniline nanocomposites

Jiang Guo[1,2] · Zhuoran Chen[2] · Waras Abdul[1] · Jie Kong[3] · Mojammel A. Khan[4] · David P. Young[4] · Jianfeng Zhu[1] · Zhanhu Guo[2]

Received: 31 December 2020 / Revised: 3 March 2021 / Accepted: 9 March 2021 / Published online: 8 April 2021

Abstract

Tunable positive magnetoresistance (MR) of polyaniline (PANI) nanocomposites with different magnetic nanoparticles (Fe_3O_4 or $CoFe_2O_4$) have been prepared through the facile surface-initiated polymerization (SIP) method. The characterizations including Fourier transform infrared (FT-IR), X-ray diffraction (XRD), scanning electron microscope (SEM), and transmission electron microscope (TEM) indicate that the magnetic nanoparticles were successfully coated by PANI. A quasi 3D variable range hopping (VRH) mechanism was observed in the magnetic PANI nanocomposites through Mott VRH model. The effects of magnetic field and magnetic nanoparticle on the charge carrier's behavior were studied by the wave function shrinkage model. The localization length and average hopping length decrease with increasing magnetic field, while the density of state at the Fermi level increases with increasing magnetic field. The enhanced dielectric property and magnetic property of the magnetic PANI nanocomposites were reported as well.

Keywords Magnetoresistance · Magnetic PANI nanocomposites · Variable range hopping mechanism

1 Introduction

Due to light weight, cost-effective processability, and unique physicochemical properties, polymer nanocomposites have spurred great interest for different applications [1–6]. Magnetoresistance (MR) is the electrical resistance change of the materials once the magnetic field is applied. The MR has great potential for many applications such as novel programmable logic devices and magnetoresistive random access memories (MRAM) [7–9]. Recently, researchers have done many works on the MR of polymer nanocomposites. For example, Zhu et al. reported the observed MR signal in magnetic carbon nanocomposite fibers [10].

Because of the low manufacturing cost, easy processability, unique mechanical flexibility, controllable electrical conductivity, and chemical functionalization capabilities, the conjugated conductive polyaniline (PANI) has attracted great attention for different applications such as energy storage, environmental remediation, antistatic or anticorrosive coating, electrochromic devices, and coupling agent [11–16]. For example, Wang et al. reported the manganese iron oxide/polyaniline nanocomposites for color switching and energy storage [12]. Gu et al. enhanced the mechanical property of silica epoxy nanocomposites with polyaniline as the coupling agent [17]. As the unique advantages of PANI, researchers have done many works about the MR of PANI nanocomposites. For example, Qiu et al. observed the MR signal in polyaniline-modified carbon fibers [13]. Gu et al.

✉ Jiang Guo
jguo@sust.edu.cn

✉ Jie Kong
kongjie@nwpu.edu.cn

✉ Zhanhu Guo
zguo10@utk.edu

[1] School of Materials Science and Engineering, Shaanxi Key Laboratory of Green Preparation and Functionalization for Inorganic Materials, Shaanxi University of Science & Technology, Xi'an 710021, China

[2] Integrated Composites Laboratory (ICL), Department of Chemical & Biomolecular Engineering, University of Tennessee, Knoxville, TN 37996, USA

[3] Shaanxi Key Laboratory of Macromolecular Science and Technology, School of Chemistry and Chemical Engineering, Northwestern Polytechnical University, Xi'an 710072, Shaanxi, China

[4] Department of Physics and Astronomy, Louisiana State University, Baton Rouge, LA 70803, USA

studied the MR in poly(p-phenylene-2,6-benzobisoxazole) short fibers/PANI nanocomposites [18].

Adding different nanofillers into the PANI matrix could change the MR signal of PANI nanocomposites, which is very important to develop the MR applications to meet the rigorous requirements in some fields. In order to study the MR behavior of polymer nanocomposites, different models have been developed including excitonic pair mechanism model, electron-hole recombination model, and bipolaron model [19–21]. Gu et al. reported the MR signal in the PANI-coated silicon nanocomposites and studied the charge carrier behavior under the magnetic field [22]. Romero et al. reported the increased amount of polarons to explain the improved negative MR in the manganite/polyaniline nanocomposites [23]. Magnetite (Fe_3O_4) and cobalt ferrite ($CoFe_2O_4$) are the traditional magnetic material used in different areas such as magnetic storage media and medical diagnostics [24, 25]. Recently, the MR of Fe_3O_4/PANI and $CoFe_2O_4$/PANI were reported; however, the loading of the Fe_3O_4 and $CoFe_2O_4$ in the PANI composites was different. Until now, there is less work about the MR of Fe_3O_4/PANI and $CoFe_2O_4$/PANI at the same loading level. And the effect of the magnetic particle's type on the MR of PANI nanocomposites is not reported [26, 27].

In this work, PANI nanocomposites with different magnetic nanoparticles (Fe_3O_4 or $CoFe_2O_4$) were synthesized by the surface-initiated polymerization (SIP) method. The permittivity as a function of frequency at room temperature, temperature-dependent resistivity, and MR of magnetic PANI nanocomposites was systematically investigated. The Mott variable range hopping (VRH) model was applied to study the electrical conduction mechanism of the magnetic PANI nanocomposites. Positive MR of the magnetic PANI nanocomposites was controlled by the magnetic nanoparticles and nanoparticle loading at room temperature. The charge carrier behavior in the magnetic PANI nanocomposites under the magnetic field was studied by the wave function shrinkage model. Meanwhile, the magnetic field's effect on the localization length, density of state at the Fermi level, average hopping length, and average hopping energy were reported. In addition, the morphology of the magnetic PANI nanocomposites were characterized by the scanning electron microscope (SEM), and the dispersion of the magnetic nanoparticle in the PANI matrix was characterized by the transmission electron microscope (TEM). The chemical structure of magnetic PANI nanocomposites was characterized by Fourier transform infrared (FT-IR). The crystallinity of the magnetic PANI nanocomposites was studied by X-ray diffraction (XRD) as well.

2 Experimental

2.1 Materials

The Fe_3O_4 and $CoFe_2O_4$ were obtained from Nanostructured & Amorphous Materials, Inc. The ammonium persulfate (APS, $(NH_4)_2S_2O_8$, 98%) and *p*-toluene sulfonic acid (PTSA, $C_7H_8O_3S$, ≥ 98.5%) and aniline (C_6H_7N, 99.0%) were purchased from Fisher Scientific. All the chemicals were used as-received without any further treatment.

2.2 Fabrication of magnetic PANI nanocomposites

The magnetic (Fe_3O_4 or $CoFe_2O_4$)/PANI nanocomposites were fabricated a facial surface-initiated polymerization method. Firstly, the magnetic nanoparticles were dispersed in the aqueous solution containing PTSA (30 mmol) and APS (18 mmol) in 200 mL deionized water treated by 60-min sonication and mechanical stirring (SCILOGEX OS20-Pro LCD Digital Overhead Stirrer, 300 rpm) in an ice-water bath. Secondly, the aniline solution (36 mmol, 50 mL deionized water) was mixed with the magnetic nanomaterial suspension and mechanically and ultrasonically stirred continuously for additional 120 min in the ice water bath for polymerization. Thirdly, the product was vacuum filtered and washed with deionized water several times to remove any unreacted PTSA and APS, then washed with ammonia solution to de-dope the PANI nanocomposites, then redoped with 1 M PTSA solution. The final synthesized nanocomposites were dried at 50°C in oven overnight. The Fe_3O_4/PANI nanocomposites with a Fe_3O_4 loading of 20.0 and 40.0% were synthesized, and $CoFe_2O_4$/PANI nanocomposites with a $CoFe_2O_4$ loading of 20.0 and 40.0 wt% were synthesized as well. Pure PANI was fabricated following the above procedures without adding any nanoparticles for comparison.

2.3 Characterizations

The morphology of the as-synthesized materials was examined by a FEI Helios NanoLab 600i scanning electron microscopy (SEM, Hillsboro, OR). All the samples were sputter coated with a thin layer of carbon (about 3 nm) to ensure good imaging. The FT-IR spectra of the products were obtained on a Nicolet IS 10 (in the range from 650 to 2000 cm^{-1} at a resolution of 4 cm^{-1}). The XRD was measured by D/max-rB wide-angle X-ray diffractometer at a Cu k_α wavelength of 0.154 nm. The scanning rate is 4° min^{-1} from 10 to 80°. Dielectric properties were investigated by a LCR meter (Agilent, E4980A) equipped with a dielectric test fixture (Agilent, 16451B) at the frequency of 20 to 2×10^6 Hz at room temperature. The pure PANI and magnetic/PANI nanocomposites were pressed in a form of disk

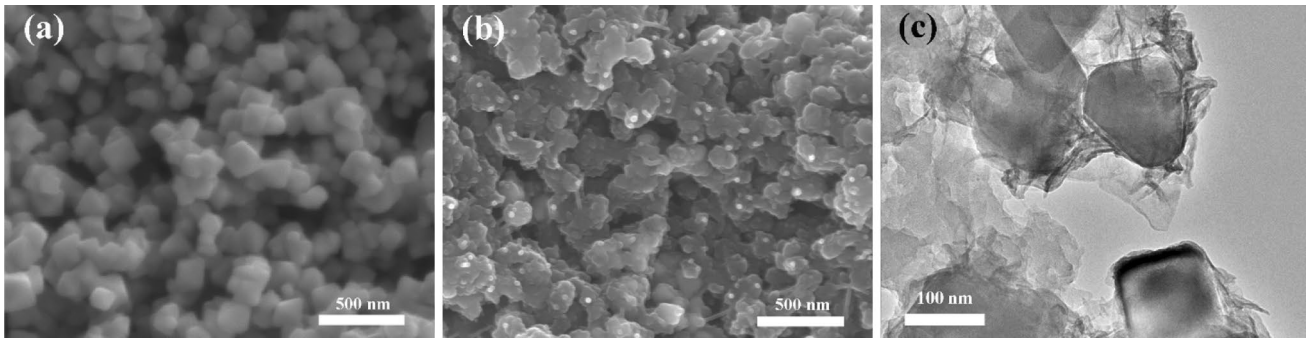

Fig. 1 **(a)** SEM image of pure Fe_3O_4, **(b)** SEM image of 20.0 wt% Fe_3O_4/PANI, and **(c)** TEM image of 20.0 wt% Fe_3O_4/PANI

pellet with a diameter of 25 mm by a hydraulic presser. The same samples were also used to measure the resistivity and MR. The temperature-dependent resistivity was measured by a standard four-probe method from 50 to 290 K. The MR measurement of the PANI nanocomposites was carried out using a standard four-probe technique by a 9-T Physical Properties Measurement System (PPMS) by Quantum Design at 290 K. The magnetic properties were also investigated in the 9-T PPMS by Quantum Design.

3 Results and discussion

3.1 SEM and TEM

Figure 1 displays the SEM images of pure Fe_3O_4 nanoparticles and 20.0 wt% Fe_3O_4/PANI nanocomposites and TEM image of 20.0 wt% Fe_3O_4/PANI nanocomposites. The surface of pure Fe_3O_4 is very smooth, and the Fe_3O_4 shows cubic shape (Fig. 1a). For the Fe_3O_4 coated by PANI, the surface of the nanoparticle is rougher which is due to the coating of PANI on Fe_3O_4 (Fig. 1b). The same result is observed in the 20.0 wt% $CoFe_2O_4$/PANI nanocomposites (Fig. S1c). Figure 1c shows the TEM image of 20.0 wt% Fe_3O_4/PANI nanocomposites; it is obviously observed that Fe_3O_4 nanoparticles are dispersed in the PANI matrix, which further confirms that nanoparticle is coated by PANI through the SIP method.

3.2 XRD analysis

Figures 2 and S2 display the XRD curves of the pure Fe_3O_4, $CoFe_2O_4$, pure PANI, and magnetic $CoFe_2O_4$/PANI and Fe_3O_4/PANI. There are only two board diffraction peaks located at 20.01 and 25.16° observed in pure PANI, corresponding to (100) and (110) crystallographic planes of the partially crystalline PANI [28] (Fig. S2). For pure $CoFe_2O_4$, the peaks located at 35.5, 37.1, 43.1, 53.1, 57.1, and 62.7° correspond to (311), (222), (400), (422), (511), and (440) crystallographic planes

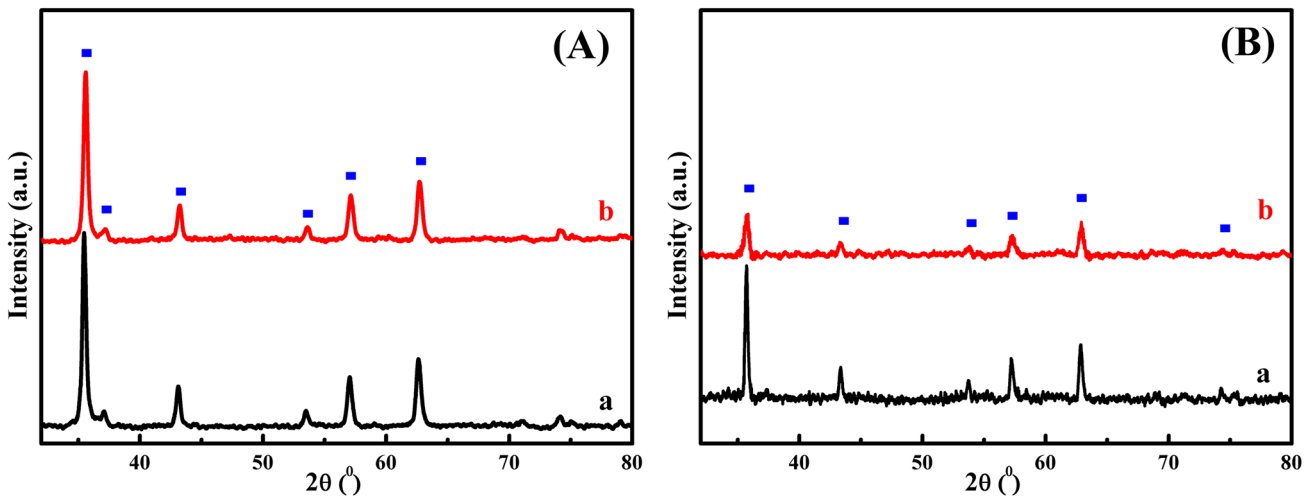

Fig. 2 XRD patterns of **(A)** **(a)** pure $CoFe_2O_4$ and **(b)** 20.0 wt% $CoFe_2O_4$/PANI, **(B)** **(a)** pure Fe_3O_4 and **(b)** 20.0 wt% Fe_3O_4/PANI

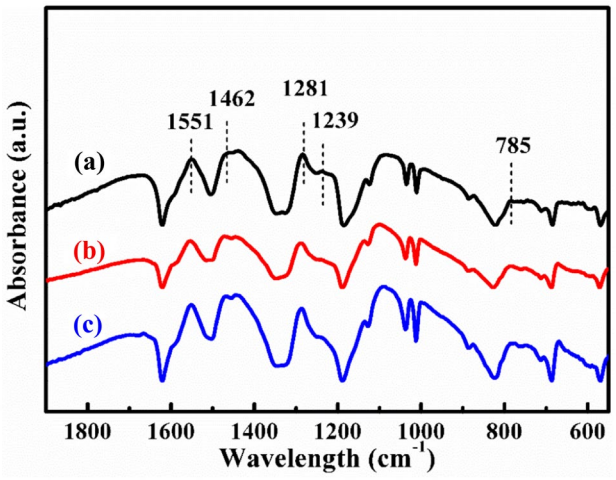

Fig. 3 FT-IR spectra of **(a)** PANI, **(b)** 20.0 wt% Fe_3O_4/PANI, and **(c)** 20.0 wt% $CoFe_2O_4$/PANI

of $CoFe_2O_4$, respectively (Fig. 2A(a)). The observed characteristic peaks were indexed to the face-centered cubic crystal structure of $CoFe_2O_4$ [29]. Meanwhile, these characteristic peaks of $CoFe_2O_4$ are observed in the 20.0 wt% $CoFe_2O_4$/PANI nanocomposites (Fig. 2A(b)). There are 6 characteristic peaks observed in the pure Fe_3O_4 (Fig. 2B(a)). The peaks located at $2\theta = 35.7$, 43.3, 53.7, 57.2, 63.3, and 74.3° in the XRD curve of Fe_3O_4 correspond to (311), (400), (422), (511), (400), and (533) crystallographic planes of the spinel phase of Fe_3O_4, respectively [30]. The characteristic peaks of Fe_3O_4 are observed in the Fe_3O_4/PANI nanocomposites as well.

3.3 FT-IR analysis

Figure 3 shows the FT-IR spectra of pure PANI and 20 wt% Fe_3O_4/PANI and 20.0 wt% $CoFe_2O_4$/PANI nanocomposites. For pure PANI (Fig. 3a), the peak located at 785 cm^{-1} is due to the out-of-plane vibration of C–H in the substituted benzenoid ring [31]. The peak at 1239 cm^{-1} is attributed to the C–H in-plane vibration of the quinoid unit [31]. And the peak at 1281 cm^{-1} corresponds to the C–N stretching vibration of the benzenoid unit [11]. The peaks located at 1551 and 1462 cm^{-1} correspond to the characteristic C = C stretching vibration of the quinoid and benzenoid rings, indicating the oxidation state of emeraldine salt state in the PANI [28, 32]. The characteristic peaks of PANI are also observed in PANI nanocomposites with different magnetic nanoparticles (Fig. 3b, c and Fig. S3). Meanwhile, compared with pure PANI, the characteristic peaks of magnetic PANI nanocomposites have a little shift, indicating the interaction between PANI and the nanoparticles. The morphological analysis from SEM and TEM images, crystal structure analysis from XRD, and chemical structure analysis from FT-IR indicate that the PANI nanocomposites with different magnetic nanoparticles (Fe_3O_4 or $CoFe_2O_4$) were successfully fabricated by the SIP method.

3.4 Dielectric property

Figure 4A displays the real permittivity ε' as a function of frequency for pure PANI, 20 wt% Fe_3O_4/PANI, and 20.0 wt% $CoFe_2O_4$/PANI nanocomposites at room temperature. For all the fabricated samples, the ε' decreases with increasing frequency (Fig. 4A). Normally, due to the electric leakage,

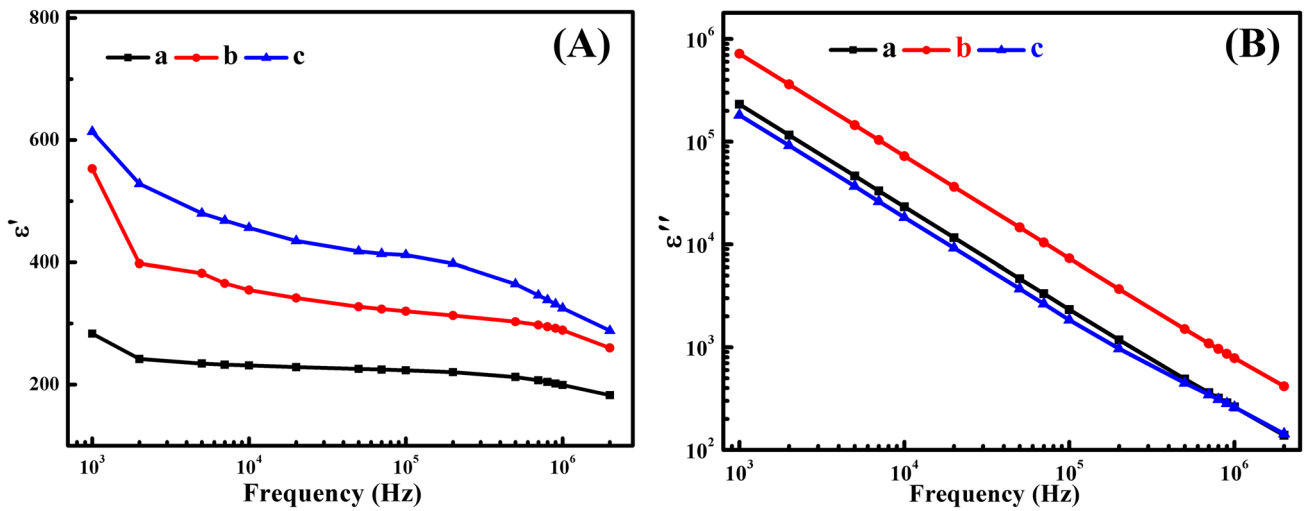

Fig. 4 **(A)** Real permittivity of **(a)** pure PANI, **(b)** 20.0 wt% Fe_3O_4/PANI, and **(c)** 20.0 wt% $CoFe_2O_4$/PANI. **(B)** Imaginary permittivity of **(a)** pure PANI, **(b)** 20.0 wt% Fe_3O_4/PANI, and **(c)** 20.0 wt% $CoFe_2O_4$/PANI

the ε' of dielectric medium decreases with increasing frequency [33]. For pure PANI (Fig. 4A(a)), the ε' decreases from 283.51 to 182.67 within the measured frequency. The ε' decreases sharply from 1×10^3 to 1×10^4 Hz, which is due to the Maxwell-Wagner-Sillars polarization effect. For the Maxwell-Wagner-Sillars polarization effect, the charge carriers are accumulated at the internal interfaces or at the external electrode-sample interface on a macroscopic scale under the electrical field [34]. After that, the ε' decreases slowly with increasing the frequency. At higher frequency, the decreasing of ε' is due to the "delay" of the polarization of charge carrier in response to the changing electric field. The magnetic PANI nanocomposites show ε' higher than pure PANI, which is due to the more interface areas formed between polymer and nanoparticles in the PANI nanocomposites [1, 30]. Figure 4B shows the imaginary permittivity ε'' of pure PANI, 20 wt% Fe_3O_4/PANI, and 20.0 wt% $CoFe_2O_4$/PANI nanocomposites. For all the samples, with increasing the frequency, the ε'' decreases in the measured frequency range at room temperature. The 20.0 wt% Fe_3O_4/PANI nanocomposites show higher ε'' pure PANI and 20.0 wt% $CoFe_2O_4$/PANI, indicating a higher dielectric loss which may be due to the conduction loss and polarization loss [35, 36].

3.5 Electrical conductivity

The temperature-dependent resistivity of pure PANI, 20.0 wt% Fe_3O_4/PANI, and 20.0 wt% $CoFe_2O_4$/PANI nanocomposites were measured from 150 to 290 K to determine the electrical conduction mechanism. In Fig. 5A, the resistivity of all the samples decrease with increasing the temperature, indicating a typical behavior of semiconductor [35]. The magnetic PANI nanocomposites show relatively larger resistivity than pure PANI. This is because the insulated magnetic particles deteriorated the electrical conduction network of PANI and impeded the movement of charge carriers. And the resistivity of $CoFe_2O_4$/PANI is larger than that of Fe_3O_4/PANI at the same particle loading level (Fig. 5A). Therefore, the resistivity of the PANI could be adjusted by the assistance of the magnetic nanoparticles. For the conjugated conductive polymers, the behavior of charge carriers depends on the amount of disorder including variations in conjugation length, rotations, and kinking of polymer chain interaction with neighboring molecules, impurities, and dipoles from residual solvent molecules [35, 37]. Normally, resistivity ratio (ρ_r, $\rho_r = \rho_{150}/\rho_{290}$) can be used to express the disorder for conductive polymers [28, 30]. The calculated disorder for pure PANI, 20.0 wt% Fe_3O_4/PANI, and 20.0 wt% $CoFe_2O_4$/PANI nanocomposites is summarized in Table 1. Compared with pure PANI, the 20.0 wt% Fe_3O_4/PANI and 20.0 wt% $CoFe_2O_4$/PANI show higher disorder degree. The adding of magnetic nanoparticles affects the disorder of PANI matrix.

For pure PANI, 20.0 wt% Fe_3O_4/PANI, and 20.0 wt% $CoFe_2O_4$/PANI nanocomposites, the Mott variable range hopping (VRH) model is applied to study the electron transport mechanism [38] and represented as Eq. 1

Table 1 ρ_r, σ_0, and T_0 for the pure PANI and magnetic PANI nanocomposites with different magnetic nanoparticles

Sample	ρ_r	σ_0 (S cm^{-1})	$T_0\times10^5$ (K)
Pure PANI	4.31	1705.1	28.00
20 wt% Fe_3O_4/PANI	6.94	59,655.4	89.81
20 wt% $CoFe_2O_4$/PANI	6.88	17,777.7	88.36

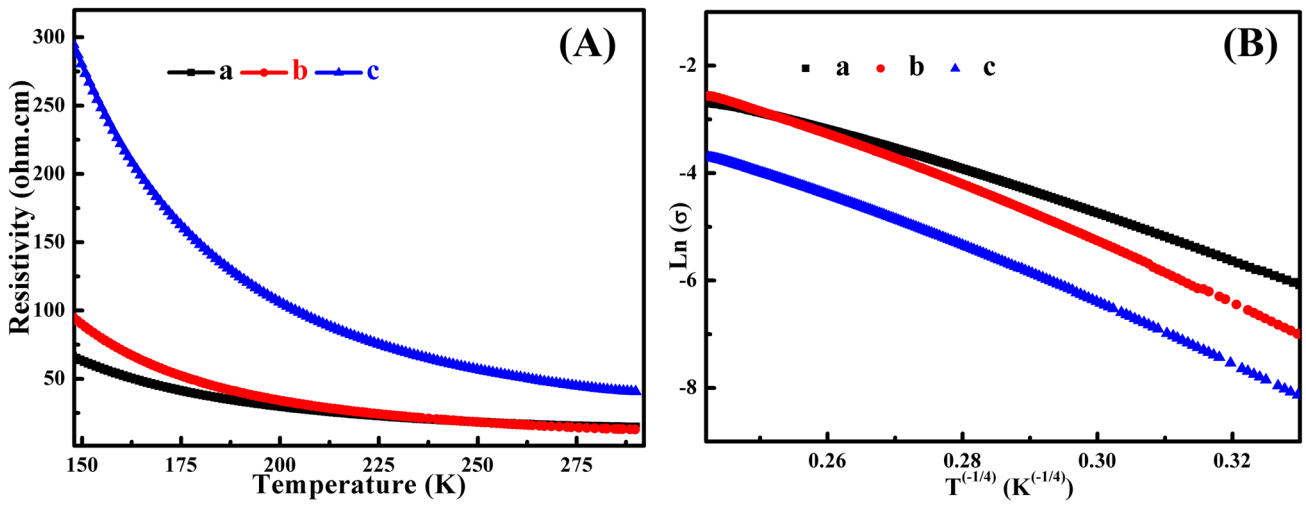

Fig. 5 **(A)** Temperature-dependent resistivity of **(a)** pure PANI, **(b)** 20.0 wt% Fe_3O_4/PANI, and **(c)** 20.0 wt% $CoFe_2O_4$/PANI. **(B)** ln(σ) as a function of $T^{-1/4}$ of **(a)** pure PANI, **(b)** 20.0 wt% Fe_3O_4/PANI, and **(c)** 20.0 wt% $CoFe_2O_4$/PANI

$$\sigma = \sigma_0 \exp\left[-\left(\frac{T_0}{T}\right)^{1/1+n}\right] n = 1,\ 2,\ 3 \quad (1)$$

where the n value of 3, 2, and 1 is for three-, two-, and one-dimensional systems, respectively [39]. The pre-exponential factor σ_0 is constant which represents the conductivity at infinite low temperature limit. T is the Kelvin temperature (K), and T_o is the characteristic Mott temperature (K) and expressed as Eq. 2 [40]:

$$T_0 = 24/[\pi k_B N(E_F) a_0^3] \quad (2)$$

where a_o, k_B, and $N(E_F)$ stand for the localization length of the localized wave function of charge carriers, Boltzmann constant, and the density of states at the Fermi level, respectively [39]. Normally, T_o is related to the localization length and the density of states at the Fermi level. The Eq. 1 can be rearranged to Eq. 3:

$$\ln \sigma = \ln \sigma_0 - \left(\frac{T_0}{T}\right)^{1/1+n} \quad n = 1,\ 2,\ 3 \quad (3)$$

So, σ_0 and T_0 can be obtained from the intercept and slope of the plot of ln $(\sigma) \sim T^{-1/(1+n)}$, respectively. The plot of ln $(\sigma) \sim T^{-1/(1+n)}$ for all the samples is shown in Fig. 5B. The pure PANI, 20.0 wt% Fe_3O_4/PANI, and 20.0 wt% $CoFe_2O_4$/PANI nanocomposites follow a ln $(\sigma) \sim T^{-1/4}$ linear relationship, which indicates a quasi 3D VRH electrical conduction mechanism. The calculated σ_0 and T_0 values are summarized in Table 1. The T_0 of pure PANI is lower than that of magnetic PANI nanocomposites. Generally, the T_o is strongly dependent on the disorder of PANI, which means the random sequence of quinoid-benzenoid groups in PANI presented in the samples [41, 42]. The T_o displays the same trend as ρ_r as observed in Table 1.

3.6 Magnetic property

Magnetization (M) is a phenomenon that describes the response of the magnetic materials to an external magnetic field. The magnetic domains separated by the domain walls are responsible for the magnetic behavior of the ferromagnetic material [43]. Because of the unpaired electrons, the atoms have net magnetic moment formed by the exchange interaction in the ferromagnetic material. In a single magnetic domain, the atoms' magnetic moment is aligned parallel in the same direction. The magnetic domains are randomly organized without the applied magnetic field. Once the magnetic field applied, the magnetic moment in these domains will be aligned in the same direction, and the alignment depends on the strength of the applied magnetic field [44]. This is the magnetization process of the ferromagnetic material, and the magnetization increases with increasing the magnetic field until it reaches the saturation magnetization (M_s) [30]. Figure 6 shows the magnetization curves of the pure magnetic nanoparticles and the magnetic PANI nanocomposites at room temperature. The remanence (the magnetization left behind in the ferromagnetic material when the applied magnetic field becomes 0 H) of pure Fe_3O_4 is 9.0 emu/g (Fig. 6A(a)); then, the remanence decreases to 2.5 emu/g for 20.0 wt% Fe_3O_4/PANI nanocomposites (Fig. 6A(b)). Normally, coercivity of magnetic material greater than 200 Oe is defined as ferromagnetic hard, while coercivity smaller than 200 Oe is defined as ferromagnetic soft

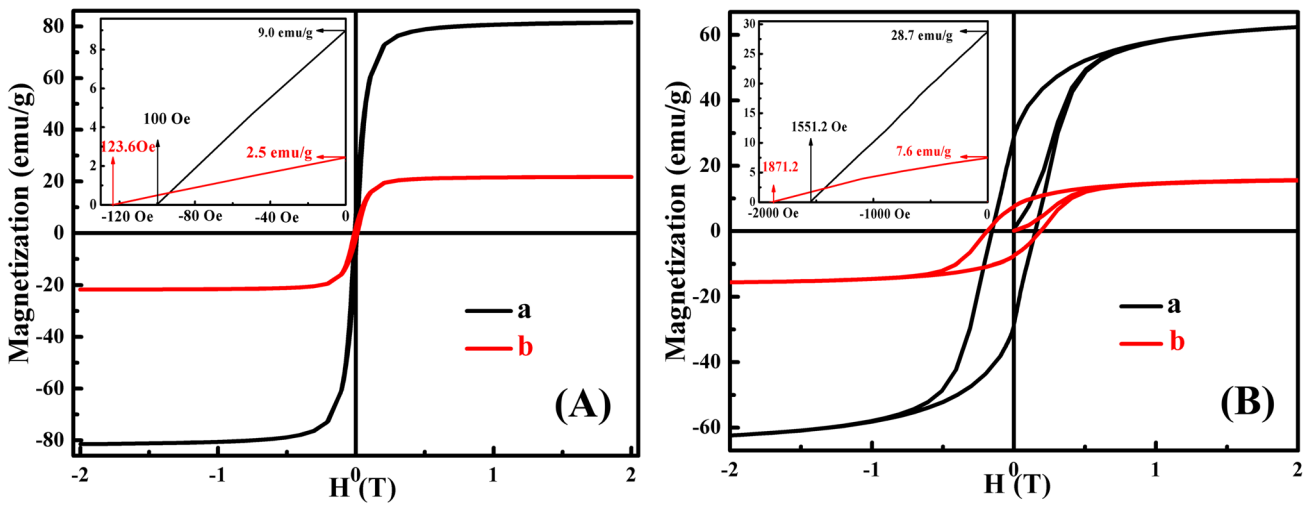

Fig. 6 Room temperature magnetization as a function of magnetic field for **(A)** **(a)** pure Fe_3O_4 and **(b)** 20.0 wt% Fe_3O_4/PANI; **(B)** **(a)** pure $CoFe_2O_4$ and **(b)** 20.0 wt% $CoFe_2O_4$/PANI

[45]. It is obvious that the coercivity of pure Fe_3O_4 and 20.0 wt% Fe_3O_4/PANI is smaller than 200 Oe indicating that these two materials are ferromagnetic soft (Fig. 6A). However, the coercivity of pure $CoFe_2O_4$ and 20.0 wt% $CoFe_2O_4$/PANI is greater than 200 Oe, reflecting the ferromagnetic hard materials (Fig. 6B). Compared with pure magnetic nanoparticles (Fe_3O_4 and $CoFe_2O_4$), the Fe_3O_4/PANI and $CoFe_2O_4$/PANI nanocomposites show greater coercivity. It can be concluded that the coercivity of the magnetic nanoparticles can be controlled by the PANI modification through the SIP method. It is observed that the M of all the samples did not reach saturation within the measured magnetic field. The M_s could be determined by the extrapolated M_s obtained from the intercept of $M \sim H^{-1}$ at high magnetic field [1]. The obtained M_s of Fe_3O_4 and $CoFe_2O_4$ are 82.75 and 67.05 emu/g, respectively. The calculated M_s of 20.0 wt% Fe_3O_4/PANI and 20.0 $CoFe_2O_4$/PANI nanocomposites are 21.93 and 16.75 emu/g. Based on the results of M_s, the weight percent of magnetic PANI nanocomposites could be calculated. The calculated weight percent of 20.0 wt% Fe_3O_4/PANI and 20 wt% $CoFe_2O_4$/PANI is 26.5 and 25.0%, respectively. This may be because the pyrrole monomer formed the oligomer during the polymerization [26].

3.7 Magnetoresistance

MR can be expressed by using Eq. 4:

$$\mathrm{MR}\% = \frac{R(H) - R(0)}{R(0)} \times 100 \tag{4}$$

where $R(0)$ is the resistance without magnetic field and $R(H)$ is the resistance under the magnetic field H. Positive MR are observed in all the samples and MR signal increase sharply at lower magnetic field; meanwhile, MR increases slightly at higher magnetic field (Fig. 7). The MR of pure PANI is 22.5% at 5 T (=50,000 Oe) which is higher than the magnetic PANI nanocomposites (3.4% for Fe_3O_4/PANI and 17.5% for $CoFe_2O_4$/PANI), and the MR of $CoFe_2O_4$/PANI (17.5% at 5 T) is higher than that of Fe_3O_4/PANI (3.4% at 5 T) nanocomposites at room temperature. Compared with pure PANI, the reduced MR in PANI nanocomposites indicates that magnetic nanoparticles could improve the electron transport in the PANI matrix under the external magnetic field. Generally, the wave-function shrinkage model is designed to explain the positive MR of highly disorderedly localized systems in the VRH regime [46]. Since the pure PANI and magnetic PANI nanocomposites show quasi 3D Mott VRH electrical conduction mechanism, so the wave-function shrinkage model can be used to study the MR of the pure PANI and magnetic PANI nanocomposites, and the positive MR could be expressed as Eq. 5 [28]:

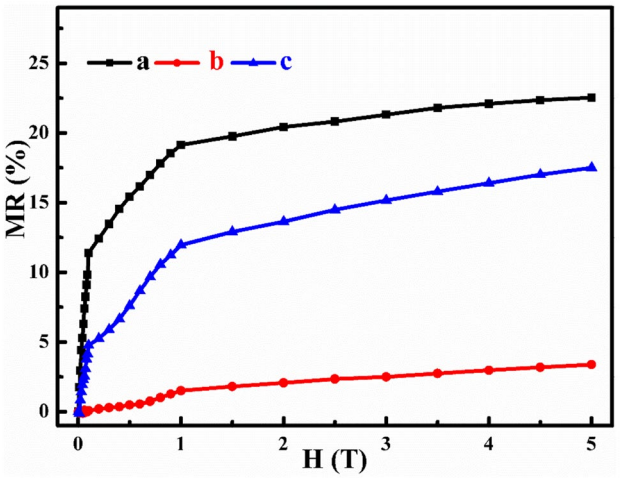

Fig. 7 MR of **(a)** pure PANI, **(b)** 20.0 wt% Fe_3O_4/PANI, and **(c)** 20.0 wt% $CoFe_2O_4$/PANI at 290 K

$$\mathrm{MR} = \frac{R(H,T) - R(0,T)}{R(0,T)} \approx t_2 \frac{H^2}{P_C^2} \left(\frac{T_0}{T}\right)^{1/4} = t_2 \frac{e^2 a_0^4}{36\hbar^2} \left(\frac{T_0}{T}\right)^{3/4} H^2 \tag{5}$$

where H, Pc, e, and h indicate the magnetic field, the fitting parameter, electron charge, and the reduced Planck's constant, respectively. And numerical constant t_2 is 5/2016. The localization length a_0 can be described as Eq. 6:

$$a_0^4 = \frac{36h^2 MR}{t_2 e^2} \left(\frac{T_0}{T}\right)^{-3/4} H^{-2} \tag{6}$$

Then, the density of states at the Fermi level $N(E_F)$ for all the samples can be calculated from Eq. 7 [30]:

$$N(E_F) = 24/[\pi k_B T_0 a_0^3] \tag{7}$$

The obtained $N(E_F)$ is summarized in Table 2 as well. Generally, the higher $N(E_F)$, the more hopping probability of charge carriers to hope between the localized states. The average hopping length R_{hop} can be calculated from Eq. 8 [39]:

$$R_{hop} = (3/8)(T_0/T)^{1/4} a_0 \tag{8}$$

The obtained a_0, $N(E_F)$, and R_{hop} are summarized in Table 2. For all the samples, the a_0 and R_{hop} decrease with increasing the magnetic field, while the $N(E_F)$ increases with increasing the magnetic field. For pure PANI, the charge carrier could hop between the "metallic islands" in the PANI matrix**.** As a half-metallic ferromagnetic material, Fe_3O_4 is a promising material to serve as a spin-polarized electron source [47, 48]. In the 20.0 wt% Fe_3O_4/PANI nanocomposites, the Fe_3O_4 nanoparticles can form a spin-polarized current under the magnetic field,

Table 2 The calculated a_o, $N(E_F)$, and R_{hop} for the pure PANI, 20.0 wt% Fe_3O_4/PANI, and 20.0% $CoFe_2O_4$/PANI nanocomposites

Sample	Parameters	Magnetic field (T)		
		1	2	5
Pure PANI	a_0 (nm)	33.34	23.96	15.53
	$N(E_F)$ ((J cm^3)$^{-1}$)	5.33×10^{33}	1.44×10^{34}	5.27×10^{34}
	R_{hop} (nm)	123.94	89.07	57.74
20 wt% Fe_3O_4/PANI	a_0 (nm)	14.19	10.86	7.77
	$N(E_F)$ ((J cm^3)$^{-1}$)	2.15×10^{34}	4.81×10^{34}	1.31×10^{35}
	R_{hop} (nm)	70.61	54.04	38.65
20 wt% $CoFe_2O_4$/PANI	a_0 (nm)	23.9	17.46	12.3
	$N(E_F)$ ((J cm^3)$^{-1}$)	4.57×10^{33}	1.18×10^{34}	3.36×10^{34}
	R_{hop} (nm)	118.42	86.52	60.95

which increases with increasing the magnetic field strength [43]. Therefore, an increased electrical conductivity should be achieved, and a decreased positive MR is observed in 20.0 wt% Fe_3O_4/PANI nanocomposites. However, the MR of 20.0 wt% Fe_3O_4/PANI nanocomposites still increases with increasing magnetic field; this is due to the decreasing of localization length and average hopping length for the charge carrier with increasing magnetic field strength in the PANI matrix. The MR of 20.0 wt% $CoFe_2O_4$/PANI nanocomposites is higher than that of 20.0 wt% Fe_3O_4/PANI nanocomposites, but still lower than that of pure PANI, which may be due to less-generated spin-polarized electrons from $CoFe_2O_4$ in comparison with Fe_3O_4. When the nanoparticle loading further increased to 40.0 wt%, the increased positive MR is achieved in the 40.0 wt% $CoFe_2O_4$/PANI nanocomposites, as observed in Fig. S4.

4 Conclusion

The results of SEM, TEM, FT-IR, and XRD indicate that the magnetic PANI nanocomposites have been successfully synthesized. For the samples, the resistivity decreases with increasing temperature exhibiting a semiconducting behavior. And a quasi 3D VRH mechanism is observed in the Fe_3O_4/PANI and $CoFe_2O_4$/PANI through Mott VRH model. The positive MR is observed in all the PANI nanocomposites, and the MR signal is controlled by the type of magnetic particles. For the positive MR, with increasing the magnetic field, the localization length and average hopping distance decrease, while the density of state at Fermi level decreases. The enhanced dielectric property is observed in the magnetic PANI nanocomposites.

Supplementary Information The online version contains supplementary material available at https://doi.org/10.1007/s42114-021-00242-z.

Acknowledgements The project is supported by the Research Starting Foundation of Shaanxi University of Science and Technology, and Research Starting Foundation of University of Tennessee, the Research Foundation for Thousand Young Talent Plan of Shaanxi province of China.

Declarations

Conflict of interest The authors declare that they have no conflict of interest.

References

1. Guo J, Song H, Liu H, Liu X, Luo C, Zhang X, Jie K, Gou Z, Ren Y, Ding T, Khan MA, Young DP (2017) Polypyrrole-interface-functionalized nano-magnetite epoxy nanocomposites as electromagnetic wave absorbers with enhanced flame retardancy. J Mater Chem C 5:5334–5344
2. Lv L, Liu J, Liang C, Gu J, Wujcik EK (2018) An overview of electrically conductive polymer nanocomposites toward electromagnetic interference shielding. Eng Sci 2:26–42
3. Su T, Shao Q, Qin Z, Guo Z, Wu Z (2018) Role of interfaces in two-dimensional photocatalyst for water splitting. ACS Catal 8(3):2253–2276
4. Zhang K, Li GH, Feng LM, Wang N, Guo J, Sun K, Wang M (2017) Ultralow percolation threshold and enhanced electromagnetic interference shielding in poly(l-lactide)/multi-walled carbon nanotube nanocomposites with electrically conductive segregated networks. J Mater Chem C 5(36):9359–9369
5. Cai J, Wang W, Xie W, Wei X, Guo Z (2020) Carbon microfibers with tailored surface functionalities supporting iron/nickel bisalloy for highly efficient hexavalent chromium recovery. Carbon 168:640–649
6. Liu H, Huang W, Yang X, Dai K, Zheng G, Liu C, Shen C, Yan X, Guo J, Guo Z (2016) Organic vapor sensing behaviors of conductive thermoplastic polyurethane–graphene nanocomposites. J Mater Chem C 4:4459–4469
7. Ney A, Pampuch C, Koch R, Ploog KH (2003) Programmable computing with a single magnetoresistive element. Nature 425(6957):485
8. Moodera JS, Leclair P (2003) Spin electronics: a quantum leap. Nat Mater 2(11):707
9. Ikeda S, Hayakawa J, Lee YM, Matsukura F, Ohno Y, Hanyu T, Ohno H (2007) Magnetic tunnel junctions for spintronic memories and beyond. IEEE Trans Electron Devices 54:991–1002
10. Zhu J, Chen M, Qu H, Wei H, Guo J, Luo Z, Haldolaarachchige N, Young DP, Wei S, Guo Z (2013) Positive and negative magnetoresistance phenomena observed in magnetic electrospun polyacrylonitrile-based carbon nanocomposite fibers. J Mater Chem C 2:715–722
11. Guo J, Long J, Ding D, Wang Q, Shan Y, Umar A, Zhang X, Weeks BL, Wei S, Guo Z (2016) Significantly enhanced mechanical and electrical properties of epoxy nanocomposites reinforced with low loading of polyaniline nanoparticles. RSC Adv 6(25):21187–21192
12. Guo Z, Wang Y, Wei H, Liu J, Wang J, Guo J et al (2015) Electropolymerized polyaniline/manganese iron oxide hybrids with an enhanced color switching response and electrochemical energy storage. J Mater Chem A 3:3989–3998

13. Qiu B, Guo J, Wang Y et al (2015) Dielectric properties and magnetoresistance behavior of polyaniline coated carbon fabrics. J Mater Chem C 3(16):3989–3998
14. Gu H, Zhang H, Gao C, Liang C, Gu J, Guo Z (2018) New functions of polyaniline. ES Mater Manuf 1:3–12
15. Li X, Wen Z, Yin R, Huang X, Qian L (2018) A highly porous polyaniline-graphene composite used for electrochemical supercapacitors. Eng Sci 3:89–95
16. Xu X, Fu Q, Gu H, Guo Y, Guo Z (2019) Polyaniline crystalline nanostructures dependent negative permittivity metamaterials. Polymer 188:122129
17. Gu H, Guo J, Wei H, Yan X, Ding D, Zhang X, Guo Z (2015) Transparent anhydride–cured epoxy nanocomposites reinforced with polyaniline stabilized nanosilica. J Mater Chem C 3(31):8152–8165
18. Gu H, Xu X, Cai J, Wei S, Wei H, Liu H et al (2019) Controllable organic magnetoresistance in polyaniline coated poly(p-phenylene-2,6-benzobisoxazole) short fibers. Chem Commun 55:10068–10071
19. Bin H, Yue W (2007) Tuning magnetoresistance between positive and negative values in organic semiconductors. Nature 6(12):985–991
20. Kasem KK, Worley H, Elmasry M (2018) Optical and photoelectrochemical studies on photoactive inorganic/organic/organic/interface assemblies of CdS/poly 3-(2-thienyl) aniline/poly 2,2 bithiophene. Adv Compos Hybrid Mater 1:748–758
21. Prigodin VN, Bergeson JD, Lincoln DM, Epstein AJ (2006) Anomalous room temperature magnetoresistance in organic semiconductors. Synth Met 156(9–10):757–761
22. Gu H, Guo J, Sadu R, Huang Y, Haldolaarachchige N, Chen D et al (2013) Separating positive and negative magnetoresistance for polyaniline-silicon nanocomposites in variable range hopping regime. Appl Phys Lett 102(21):212403–1–212403–4
23. Romero M, Faccio R, Pardo H, Tumelero MA, Montenegro B, Campos C et al (2015) Effect of manganite nanoparticles addition in the low field magnetoresistance of polyaniline. J Mater Chem C 3:12040–12047
24. Gu H, Zhou X, Lyu S, Pan D, Guo Z (2019) Magnetic nanocellulose-magnetite aerogel for easy oil adsorption. J Colloid Interface Sci 560:849–856
25. Kim YI, Kim D, Lee CS (2003) Synthesis and characterization of CoFe2O4 magnetic nanoparticles prepared by temperature-controlled coprecipitation method. Phys B 337(1–4):42–51
26. Gu H, Zhang H, Lin J et al (2018) Large negative giant magnetoresistance at room temperature and electrical transport in cobalt ferrite-polyaniline nanocomposites. Polymer 142:324–330
27. Gu H, Huang Y, Zhang X, Wang Q, Zhu J, Shao L et al (2012) Magnetoresistive polyaniline-magnetite nanocomposites with negative dielectrical properties. Polymer 53(3):801–809
28. Guo J, Guan L, Wei H, Khan MA, Zhang X, Li B et al (2016) Enhanced negative magnetoresistance with high sensitivity of polyaniline interfaced with nanotitania. J Electrochem Soc 163(8):H664–H671
29. Adak NC, Chhetri S, Murmu NC, Samanta P, Kuila T (2019) Analytical and experimental investigation on magnetorheological behavior of $CoFe_2O_4$-rgo-incorporated epoxy fluid composites. Adv Compos Hybrid Mater 2:266–278
30. Guo J, Gu H, Wei H, Zhang Q, Haldolaarachchige N, Li Y et al (2013) Magnetite–polypyrrole metacomposites: dielectric properties and magnetoresistance behavior. J Phys Chem C 117(19):10191–10202
31. Hu Q, Sun D, Ma Y, Qiu B, Guo Z (2017) Conductive polyaniline nanorods enhanced methane production from anaerobic wastewater treatment. Polymer 120:236–243
32. Xie W, Shi Y, Wang Y, Zheng Y, Guo Z (2020) Electrospun iron/cobalt alloy nanoparticles on carbon nanofibers towards exhaustive electrocatalytic degradation of tetracycline in wastewater. Chem Eng J 405:126585
33. Cheng C, Fan R, Wang Z, Shao Q, Guo X, Xie P et al (2017) Tunable and weakly negative permittivity in carbon/silicon nitride composites with different carbonizing temperatures. Carbon 125:103–112
34. Cheng C, Fan R, Ren Y, Ding T, Qian L, Guo J et al (2017) Radio frequency negative permittivity in random carbon nanotubes/alumina nanocomposites. Nanoscale 9(18):5779–5787
35. Zhu J, Wei S, Zhang L, Mao Y, Ryu J, Karki AB, Guo Z (2011) Polyaniline-tungsten oxide metacomposites with tunable electronic properties. J Mater Chem 21(2):342–348
36. Wang Y, Xie W, Liu H, Gu H (2020) Hyperelastic magnetic reduced graphene oxide three-dimensional framework with superb oil and organic solvent adsorption capability. Adv Compos and Hybrid Mater 3(4):1–12
37. Blakesley JC, Neher D (2011) Relationship between energetic disorder and open-circuit voltage in bulk heterojunction organic solar cells. Phys Rev B 84(7):9226–9231
38. Zhang X, Zhu J, Haldolaarachchige N, Ryu J, Young DP, Wei S et al (2012) Synthetic process engineered polyaniline nanostructures with tunable morphology and physical properties. Polymer 53(10):2109–2120
39. Gu H, Guo J, Yan X, Wei H, Zhang X, Liu J et al (2014) Electrical transport and magnetoresistance in advanced polyaniline nanostructures and nanocomposites. Polymer 55(17):4405–4419
40. Zhang L, Tang ZJ (2004) Polaron relaxation and variable-range-hopping conductivity in the giant-dielectric-constant material $CaCu_3Ti_4O_{12}$. Phys Rev B 70(17):3352–3359
41. Galvo DS, Dos Santos DA, Laks B, De Melo CP, Caldas MJ (1989) Role of disorder in the conduction mechanism in polyanilines. Phys Rev Lett 63(7):786–789
42. Sarkar A, Ghosh P, Meikap AK, Chattopadhyay SK, Chatterjee SK, Ghosh M (2007) Direct and alternate current conductivity and magnetoconductivity of oxalic acid doped polyaniline. Solid State Commun 143(6–7):358–363
43. Guo S, Liu J, Huang Y, Khan MA, Wang X, Young DP, Wei S, Guo Z, Gu H, Guo J, Wei H (2015) Strengthened magnetoresistive epoxy nanocomposite papers derived from synergistic nanomagnetite-carbon nanofiber nanohybrids. Adv Mater 27(40):6277–6282
44. Cullity BD, Graham CD (2010) Magnetization Dynamics Introduction to Magnetic Materials, 2nd edn. John Wiley & Sons:409–438
45. He Q, Yuan T, Yan X, Luo Z, Haldolaarachchige N, Young D, Wei S, Guo Z (2014) One-pot synthesis of size- and morphology-controlled 1-d iron oxide nanochains with manipulated magnetic properties. Chem Commun 50:201–203
46. Su TI, Wang CR, Lin ST, Rosenbaum R (2002) Magnetoresistance of Al70Pd22.5Re7.5 quasicrystals in the variable-range hopping regime. Phys Rev B 66(5):340–351
47. Chapline MG, Wang SX (2006) Room-temperature spin filtering in a $CoFe_2O_4/MgAl_2O_4/Fe_3O_4$ magnetic tunnel barrier. Phys Rev B 74(1):0144181–0144188
48. Guo J, Li X, Liu H et al (2021) Tunable magnetoresistance of core-shell structured polyaniline nanocomposites with 0-, 1-, and 2-dimensional nanocarbons. Adv Compos Hybrid Mater. https://doi.org/10.1007/s42114-021-00211-6